International Journal of Minerals, Metallurgy and Materials
Volume 29, Number 2, February 2022, Page 256
https://doi.org/10.1007/s12613-021-2298-y

Effect of Al content on the reaction between Fe−10Mn−*x*Al (*x* = 0.035wt%, 0.5wt%, 1wt%, and 2wt%) steel and CaO−SiO_2−Al_2O_3−MgO slag

Huixiang Yu✉, *Dexin Yang*, *Jiaming Zhang*, *Guangyuan Qiu*, *and Ni Zhang*

School of Metallurgical and Ecological Engineering, University of Science and Technology Beijing, Beijing 100083, China
(Received: 5 February 2021; revised: 25 April 2021; accepted: 26 April 2021)

Abstract: The effect of Al content (0.035wt%, 0.5wt%, 1wt%, and 2wt%) on the composition change of steel and slag as well as inclusion transformation of high manganese steel after it has equilibrated with CaO−SiO_2−Al_2O_3−MgO slag was studied using the method of slag/steel reaction. The experimental results showed that as the initial content of Al increased from 0.035wt% to 2wt%, Al gradually replaced Mn to react with SiO_2 in slag to avoid the loss of Mn due to the reaction; this process caused both Al_2O_3 in slag and Si in steel to increase while SiO_2 and MnO in slag to reduce. In addition, the type of inclusions also evolved as the initial Al content increased. The evolution route of inclusions was MnO → MnO−Al_2O_3−MgO → MgO → MnO−CaO−Al_2O_3−MgO and MnO−CaO−MgO. The shape of inclusions evolved from spherical to irregular, became faceted, and finally transformed to spherical. The average size of inclusions presented a trend that was increasing first and then decreasing. The transformation mechanism of inclusions was explored. As the initial content of Al increased, Mg and Ca were reduced from top slag into molten steel in sequence, which consequently caused the transformation of inclusions.

Keywords: medium/high manganese steel; Al content; steel composition; slag composition; non-metallic inclusion; slag/steel reaction

1. Introduction

With the development of the automotive industry, much higher mechanical properties, such as strength and ductility [1−4], are required for automotive steels. On the other hand, reducing the weight of automobiles has become an important issue because of the increasing greenhouse gas emissions and depletion of energy sources. The addition of Al to high manganese steel not only reduces the density but also increases the stacking fault energy (SFE) of steel [5−7]. In addition, Al can also effectively suppress the delayed fracture of steel [8−10].

Compared with the works done in the field of materials, much fewer studies in the field of metallurgy have been carried out. Grajcar *et al.* [11], Gigacher *et al.* [12], and Park *et al.* [13] studied the inclusions in high manganese steel in the absence of top slag. The main types of inclusions are Al_2O_3, AlN, and $MnO{\cdot}Al_2O_3$, with some Mn (S, Se) in some inclusions. Park *et al.* [13] further studied the influence of Al content on the inclusions amount. The results showed that the volume fraction of inclusions reached the maximum when the Al content in steel was 3wt%. Xin *et al.*[14] investigated the effect of different Al contents on inclusions in master high manganese steel. Chen *et al.* [15] studied the effect of different additives, such as Mo, Cr, and rare earth elements, on the thermal conductivity of medium manganese steel. All the above studies were carried out without top slag.

Zhuang *et al.* [16] studied the inclusions in Fe−25Mn−3Si−3Al TWIP steel under the smelting conditions of induction furnace → argon oxygen decarburization (AOD) steelmaking → electroslag remelting (ESR). Peymandar *et al.* [17] performed research on the reaction between CaO−SiO_2−Al_2O_3−MgO slag and high manganese steel containing 17wt%−22wt% Mn and up to 3wt% Al, with a focus on the kinetics of the interfacial reaction; however, inclusions were not studied. Yu [18] explored the effect of adding 1wt% Al on the reaction between CaO−SiO_2−Al_2O_3−MgO refining slag and Fe−*x*Mn (*x* = 10wt%, 20wt%) steel, including composition change of steel and slag as well as inclusion transformation. Kim and Park [19] investigated the interfacial reaction between high Mn−Al alloyed steel and CaO−SiO_2−MgO−Al_2O_3 flux (initial composition, Al_2O_3 = 5wt%, MgO = 5wt%, CaO/SiO_2 = 0.5), in which the interfacial reaction kinetics and formation of solid phase in slag were considered, whereas non-metallic inclusions were not covered. Kang *et al.* [20] and Park *et al.* [21] studied the kinetics of the reduction of SiO_2 in molten mold flux by Al in high Mn−Al steel or Fe−Al melts during a continuous casting process. According to the above research studies, when a certain amount of Al exists in steel, a relatively strong reaction would occur between molten steel and top slag, whether refining slag or mold flux.

Medium/High manganese steel usually contains a certain amount of Al to either improve mechanical properties or ad-

✉ Corresponding author: Huixiang Yu E-mail: yuhuixiang@ustb.edu.cn

just the microstructure and the SFE. In addition, refining slag is essential for future commercial production of this steel grade. Therefore, the reaction between top slag and austenitic manganese steel would occur. However, very few research studies considered the effect of Al content on the slag/steel reaction of medium/high manganese steel. Thus, the effect of different Al contents on the reaction between Fe−10Mn−*x*Al steel and CaO−SiO_2−Al_2O_3−MgO refining slag with an initial Al_2O_3 content of 20wt% and basicity CaO/SiO_2 (*B*) of 4 was investigated at 1873 K in the present study.

2. Experimental

Experiments were performed in a high-temperature resistance furnace. 200 g metal materials were prepared by using electrolytic iron, electrolytic manganese, aluminum particles, and Fe−Mn−Al alloy. The Fe−Mn−Al alloy was made in a vacuum induction furnace in advance of the slag/steel equilibrium experiments, the compositions of which are as follows: Mn, 21.20wt%; Al, 3.21wt%; Si, 0.027wt%; Fe, 75.38wt%. 40 g slag materials were prepared by mixing reagent grade Al_2O_3, MgO, SiO_2, and dehydrated CaO. The compositions of the initial slag were 20% Al_2O_3 and 6% MgO with a slag basicity of 4. All the compositions in this paper are given in mass percentages unless specially stated.

According to the Al content, the experiments were divided into four groups: Nos. 1, 2, 3, and 4. Based on the Mn content of 10%, Al was added to obtain the initial contents of 0.035%, 0.5%, 1%, and 2% for Nos. 1, 2, 3, and 4, respectively. That was Fe−10Mn−*x*Al (*x* = 0.035%, 0.5%, 1%, and 2%).

The metal materials and slag materials were placed into a MgO crucible. Next, the temperature was raised to 1873 K, which was considered as the starting point of the slag/steel reaction. When the reaction ran to 30 min, the melt was stirred with molybdenum wire for better composition uniformity and kinetic conditions. After the reaction time reached 90 min (which was determined by a pre-equilibrium experiment), the MgO crucible was quickly lifted out and then water quenched. A certain time before and during the whole experiment, high purity Ar was infilled to retain good atmosphere protection.

After quenching, the chemical compositions of steel and slag samples were analyzed. The inclusions in steel were detected using an Explorer 4 analyzer (ThermoFisher Scientific, America); the accelerating voltage used for EDS analysis was 15 kV during observation of inclusions. The experimental method was described in detail in the authors' previous studies [18,22].

3. Results and discussion

3.1. Chemical compositions of steel

Chemical compositions of steel samples Nos. 1–4 are shown in Table 1. Compared with the initial Al content, the Al content after the reaction was significantly reduced. The initial content of Al had a great effect on the elemental content in the steel. The Mn content was less than 10% when the initial Al content was only 0.035%, whereas it was higher than 10% when the initial Al content increased to 0.5%, 1%, and 2%. The Si content tended to increase markedly with increasing initial Al content. The change of Al and Si content in this work is similar to that of Kim and Peymandar [17,19]. In both research studies, steel compositions during the reaction between Fe–*x*Mn–*y*Al steel and CaO−SiO_2−Al_2O_3−MgO flux were investigated. With increasing reaction time, the Al content decreased while the Si content increased quickly. In addition, the presence of both Mg and Ca in steel was detected when the initial Al content reached 0.5%, and the Mg content increased significantly as the initial Al content increased. The total oxygen content decreased notably with the increase of the initial Al content. The S content in steel was quite low, varying in the range of 0.0002%−0.0004%.

3.2. Chemical compositions of slag

Table 2 gives the chemical compositions of the slag samples. The CaO content in the slag was relatively stable in the first three groups of experiments, whereas it decreased in group No. 4. With the initial Al content increasing, the SiO_2 content exhibited an obvious downward trend, whereas the Al_2O_3 content showed an upward trend. In addition, the con-

Table 1. Chemical compositions of steel samples wt%

Experiment No.	Al	Mn	Si	Mg	Ca	S	T.O	Fe
1	0.0081	9.62	0.0037	—	—	0.0004	0.0029	Bal.
2	0.057	10.15	0.24	0.0011	<0.0005	0.0003	0.0014	Bal.
3	0.075	11.18	0.66	0.0024	<0.0005	0.0002	0.0009	Bal.
4	0.31	10.14	1.10	0.0055	0.0005	0.0003	0.0010	Bal.

Table 2. Chemical compositions of slag samples wt%

Experiment No.	CaO	SiO_2	Al_2O_3	MgO	MnO	FeO	B
Original slag	59.20	14.80	20.00	6.00	—	—	4.00
1	53.32	13.81	21.06	7.32	2.82	0.64	3.86
2	54.32	12.06	24.42	7.77	0.72	0.64	4.50
3	53.97	8.72	27.48	7.52	0.41	0.61	6.19
4	51.84	2.16	34.62	7.82	0.14	0.86	24.00

tent of MnO changed with the increase of the initial Al content, exhibiting a trend of a gradual decrease.

3.3. Analysis of inclusions

Most inclusions in the No. 1 steel sample were MnO type with a spherical shape, as shown in Fig. 1(a)–(c). Some inclusions contained small amounts of SiO_2 and MnS at the edge, as shown in Fig. 1(b) and (c).

Compared with the No. 1 steel sample, the types of inclusions in the No. 2 sample changed. The main types of inclusions were $MnO–Al_2O_3–MgO$ type. As shown in Fig. 2, the inclusions were centered with MgO and surrounded by the compound of MnO, MgO, and Al_2O_3; the shape of the inclusions was irregular.

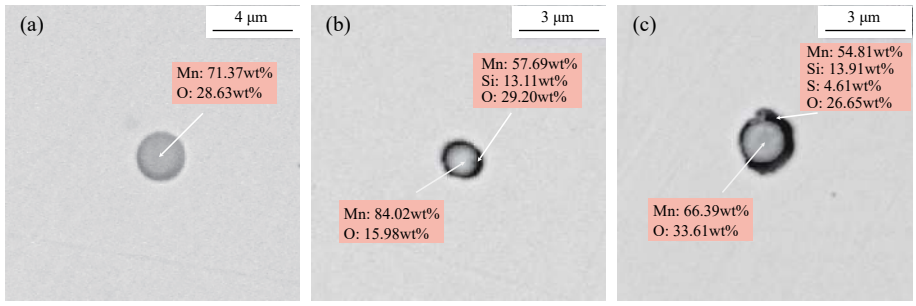

Fig. 1. Typical inclusions in No. 1 steel sample: (a) pure MnO; (b) MnO with small amounts of SiO_2; (c) MnO with small amounts of SiO_2 and MnS.

As shown in Fig. 3, the inclusions in the No. 3 steel sample transformed further. Compared with those in group No. 2, the inclusions of the No. 3 sample changed from $MnO–Al_2O_3–MgO$ type to MgO type. The type of MgO wrapped by oxide compound disappeared, and MgO became the main body of inclusions. A small amount of MnO existed in some MgO inclusions. The shape of the inclusions was faceted.

Xin *et al.* [14] studied inclusions in Fe–16Mn–*x*Al–0.6C (x = 0.002wt%, 0.033wt%, 0.54wt%, and 2.1wt%) without top slag in a MgO crucible at 1873 K. The main oxide inclusions evolved as $MnO \rightarrow Al_2O_3 \rightarrow MgAl_2O_4 \rightarrow MgO$ with increasing Al content because the dissolved Mg from the MgO crucible was reduced by Al in the liquid steel. The transformation of inclusions of steel samples No. 1 to No. 3 in the present study is similar to that of Xin's research.

For the No. 4 steel sample, there appeared another change in the inclusion types. A Ca component was detected in the inclusions. As given in Fig. 4, the types of inclusions in the No. 4 steel sample were mainly $MnO–CaO–Al_2O_3–MgO$ type and MnO–CaO–MgO type, and most inclusions were spherical in shape.

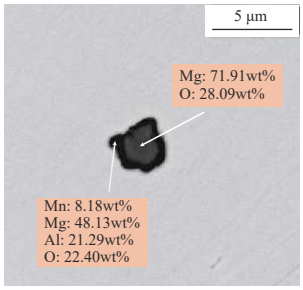

Fig. 2. Typical inclusion in the No. 2 steel sample: $MnO–Al_2O_3–MgO$.

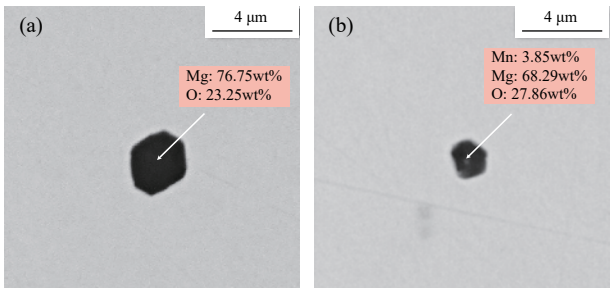

Fig. 3. Typical inclusions in the No. 3 steel sample: (a) pure MgO; (b) MgO–MnO.

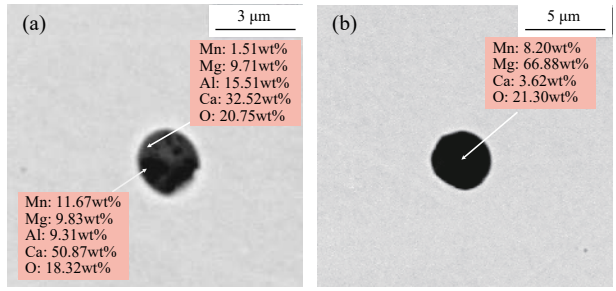

Fig. 4. Typical inclusions in the No. 4 steel sample: (a) $MnO–CaO–Al_2O_3–MgO$; (b) MnO–CaO–MgO.

The area for inclusion observation of steel samples Nos. 1, 2, 3, and 4 was 24.44, 19.72, 20.11, and 19.94 mm^2, respectively, and the numbers of detected inclusions were 159, 168, 148, and 159, respectively.

Fig. 5 shows the average contents of the observed inclusions. The compositions of inclusions varied greatly with the initial Al content. The MnO content in the inclusions decreased as the initial Al content increased. In particular, when the Al content increased from 0.035% to 0.5%, the MnO content dropped sharply from 88.63% to 21.12%. In this case, the other two main components in the inclusions were MgO and Al_2O_3. As the initial Al content increased, the MgO content in the inclusions increased first and then decreased. When the initial Al content was 1%, the types of inclusions were mainly MgO type, and the MgO content in the inclusions reached the maximum. When the initial Al content was

2%, the MgO content in the inclusions decreased. The content of Al_2O_3 in the inclusions increased when the initial Al content was less than 0.5%, decreased when Al content increased from 0.5% to 1%, and finally increased until the initial Al content reached 2%. The content of CaO in the inclusions changed little at first and then increased significantly when the initial Al content increased from 1% to 2%.

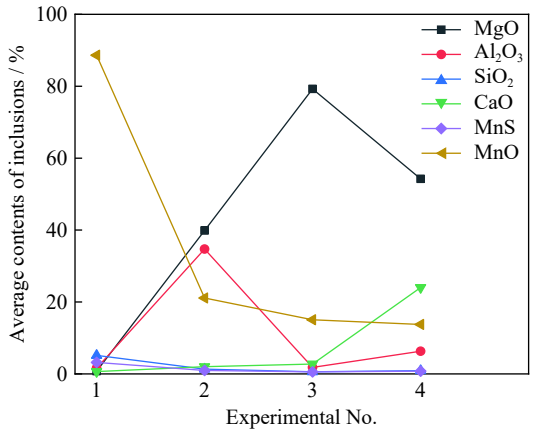

Fig. 5. Average contents of the observed inclusions.

The histogram in Fig. 6 shows the size distribution of the inclusions. The largest proportion of inclusion size in each experimental steel sample was found to be 1–2 μm. However, the ratio of inclusions in the range of 1–2 μm decreased in samples Nos. 2 and 3, whereas the ratio of inclusions of 2–3 μm and 3–4 μm increased. The size distribution of inclusions in sample No. 4 showed the opposite trend. It can be inferred that the size of the inclusions tended to increase first and then decrease as the initial Al content increased.

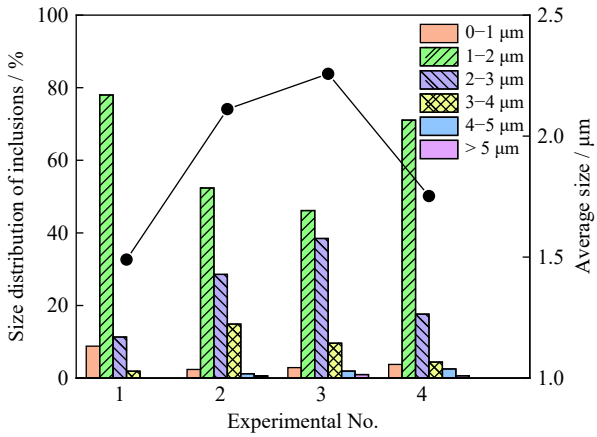

Fig. 6. Size distribution and average size of the observed inclusions.

This observation was also confirmed by the point and line chart in Fig. 6, which shows the average size change of the inclusions. The average size increased from 1.49 to 2.11 and 2.26 μm when the initial content of Al increased from 0.035% to 0.5% and 1%, respectively. However, when the Al content reached 2%, the inclusion size decreased to 1.75 μm. Interestingly, the changing trend of the average size of inclusions was consistent with that of the MgO content in the inclusions.

Fig. 7 shows the change of the inclusion shape with the increase of the initial Al content. The shape of the inclusions evolved from spherical to irregular, became faceted, and finally transformed into spherical. When the initial Al content was 0.5% or 1%, the inclusion shape was irregular. Combined with the average size change of inclusions in Fig. 6, irregular inclusions appeared to have a larger size.

Fig. 7. Change of inclusion shape.

4. Discussion

4.1. Reaction mechanism of steel and slag composition changes

Fig. 8 shows the initial and final slag compositions in the present study for different initial Al contents in the CaO−SiO_2−Al_2O_3−6%MgO multicomponent system calculated using FactSage 7.1. The compositions of the final slag in the four groups were located near the saturated line of (Ca,Mg)O, and the point of the final slag composition moved to the upper right corner; that is, as the initial Al content increased, Al_2O_3 increased and SiO_2 decreased.

The contents of Al_2O_3, SiO_2, and MnO in the final slags are shown in Table 2. As the initial content of Al increased, the Al_2O_3 content increased while the SiO_2 content decreased; this observation indicates that reaction (1) occurred during the slag/steel reaction:

$$4[Al] + 3(SiO_2) = 2(Al_2O_3) + 3[Si] \quad (1)$$

Furthermore, 2.82% MnO was formed in the experimental group with the initial Al content of 0.035%, whereas only 0.14%–0.72% MnO was formed in the other experimental groups. It can be deduced that Mn in steel mainly reacted with SiO_2 in the top slag when the initial Al content was 0.035%, as shown in reaction (2) [18]:

$$2[Mn] + (SiO_2) = 2(MnO) + [Si] \quad (2)$$

However, more Al reacted with SiO_2 in the slag as the initial Al content increased, thereby promoting reaction (1) while inhibiting reaction (2). The change of the reaction mechanism with the increase of the Al content is shown in Fig. 9. When the initial Al content was relatively low (0.035% in this study), Mn as a reducing agent reacted with SiO_2. This means that reaction (1) and reaction (2) occurred simultaneously. When the Al content increased to a high enough level (0.5% in this study), Mn is prevented from participating in the SiO_2 reduction reaction; this indicates that only reaction (1) occurred. Therefore, as the initial Al content increased, Al gradually replaced Mn as the component of the reaction with SiO_2 during the slag/steel reaction.

4.2. Evolution mechanism of the inclusions

The results from the Explorer 4 Analyzer indicate that the

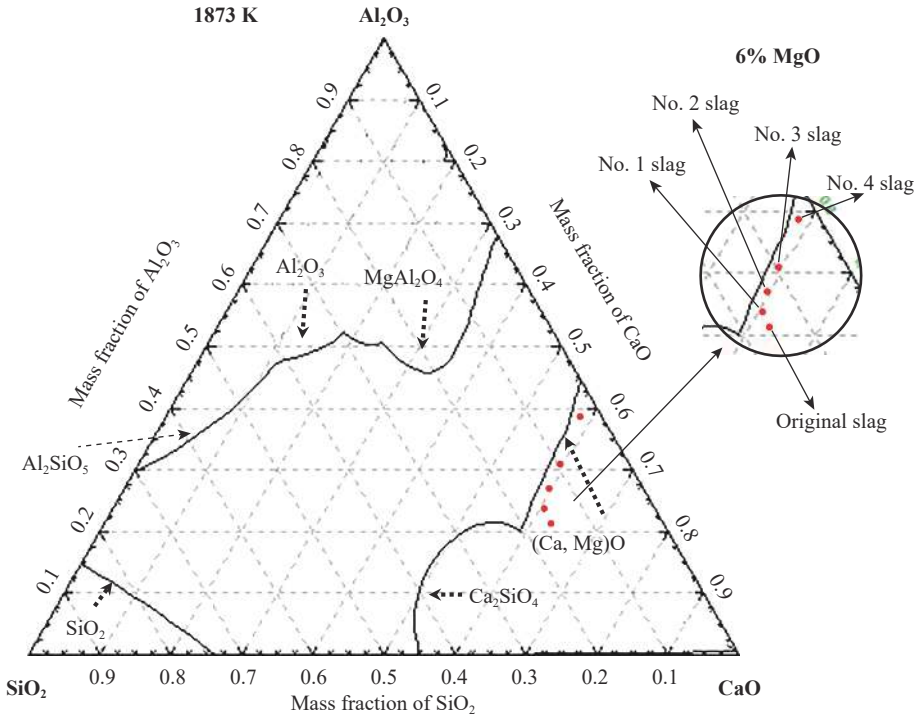

Fig. 8. Change of slag compositions with Al content at 1873 K.

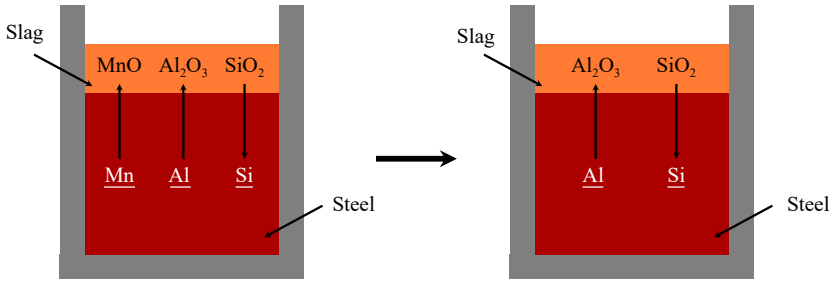

Fig. 9. Schematic of the reaction mechanism.

type of inclusions after the slag/steel reaction transformed with the increase of the initial Al content. Most inclusions observed in the No. 1 steel sample were MnO type, primarily via reaction (2) in this experimental condition, where the initial Al content was only 0.035wt%. However, the inclusions changed to MnO–Al_2O_3–MgO type in the No. 2 group with an initial Al content of 0.5wt%. Under this experimental condition, Al in the steel reacted with MgO in the slag or the MgO crucible, as shown in Eq. (3). Consequently, Mg was reduced into molten steel [23].

$$2[\mathrm{Al}] + 3(\mathrm{MgO}) = (\mathrm{Al_2O_3}) + 3[\mathrm{Mg}] \quad (3)$$

Next, the reduced Mg reacted with Al_2O_3 to form spinel, as indicated in Eq. (4) [24].

$$3[\mathrm{Mg}] + 4(\mathrm{Al_2O_3}) = 3(\mathrm{MgO \cdot Al_2O_3}) + 2[\mathrm{Al}],$$
$$\lg K_{(4)} = 34.37 - 46950/T,$$
$$K_{(4)} = \frac{a^3_{(\mathrm{MgO \cdot Al_2O_3})} \cdot a^2_{[\mathrm{Al}]}}{a^3_{[\mathrm{Mg}]} \cdot a^4_{(\mathrm{Al_2O_3})}} \quad (4)$$

where $K_{(4)}$ is the equilibrium constant of Eq. (4), $a_{[i]}$ or $a_{(i)}$ is the activity of component i in molten steel or slag, and T is the temperature.

As the initial Al content increased to 1% in the No. 3 group, more Mg was reduced by reaction (3); the reduced Mg further reacted with $MgO \cdot Al_2O_3$ to generate MgO, as shown in Eq. (5). Therefore, the type of inclusions in the No. 3 steel sample changed to MgO type.

$$3[\mathrm{Mg}] + (\mathrm{MgO \cdot Al_2O_3}) = 4(\mathrm{MgO}) + 2[\mathrm{Al}],$$
$$\lg K_{(5)} = 33.09 - 50880/T,$$
$$K_{(5)} = \frac{a^4_{(\mathrm{MgO})} \cdot a^2_{[\mathrm{Al}]}}{a^3_{[\mathrm{Mg}]} \cdot a_{(\mathrm{MgO \cdot Al_2O_3})}} \quad (5)$$

where $K_{(5)}$ is the equilibrium constant of Eq. (5).

The transformation of the inclusions was evaluated by thermodynamic calculations [18,25–26]. The formation of MgO and $MgO \cdot Al_2O_3$ inclusions was calculated. The activities of the components in steel can be expressed by Eq. (6):

$$\lg a_{[i]} = \Sigma e^j_i [\%j] + \lg[\%i] \quad (6)$$

where e^j_i is the interaction coefficient of element j to i.

The stability diagram for oxides of Al_2O_3, $MgO \cdot Al_2O_3$ and MgO can be obtained through Eqs. (4)–(6). When calculating the boundary of $MgO \cdot Al_2O_3/Al_2O_3$, the activities of $MgO \cdot Al_2O_3$ and Al_2O_3 were 0.47 and 1 respectively, while calculating the boundary of $MgO/MgO \cdot Al_2O_3$, the activities of MgO and $MgO \cdot Al_2O_3$ were 0.8 and 0.99, respectively

[27−28].

The calculated phase stability diagram for Al_2O_3, MgO·Al_2O_3 and MgO is shown in Fig. 10. The contents of dissolved [Al] and [Mg] in molten steel of the No. 2 and No. 3 experiments were near the boundary of MgO/MgO·Al_2O_3, in agreement with the result of the inclusion types observed in steel samples.

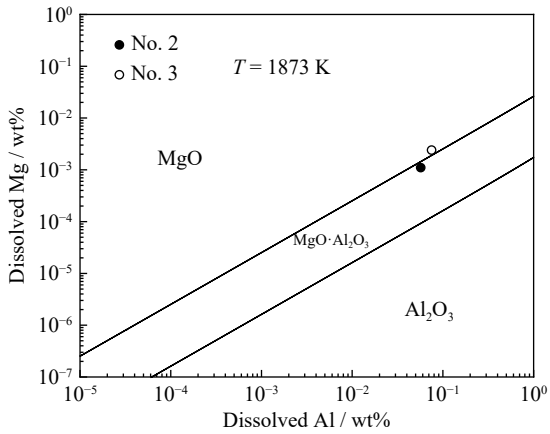

Fig. 10. Phase stability diagram of MgO/MgO·Al_2O_3/Al_2O_3.

Furthermore, in the system of very low oxygen potential, Ca could be reduced from slag by reaction (7). In the No. 4 experiment, with an initial Al content of 2%, a certain amount of Ca was detected in the steel sample, that is, the activity of Ca increased.

$$2[Al] + 3(CaO) = (Al_2O_3) + 3[Ca] \quad (7)$$

Under strong Al-deoxidation, MgO inclusions were unstable and reaction (8) would occur [29], forming a thin MgO·Al_2O_3 layer around MgO. The generated MgO·Al_2O_3 was not stable; once Ca appeared in steel, it would react with the Ca in the steel through reaction (9) [29]. Therefore, CaO−MgO−Al_2O_3 system inclusions were formed.

$$2Al^{3+} + [MgO_6]^{10-} = (MgAl_2O_4) + 2O^{2-} \quad (8)$$

$$x[Ca] + (yMgO \cdot zAl_2O_3) = (xCaO \cdot (y-x)MgO \cdot zAl_2O_3) + x[Mg] \quad (9)$$

Based on the above discussion, the transformation of the inclusions can be roughly described as follows: when the initial Al content was only 0.035%, Mn was the main reducing agent, and the inclusions in the steel were mainly MnO. When the initial Al content reached 0.5%, Al gradually became the main reducing agent, reducing Mg from MgO in the slag or the crucible; thus, a large amount of MgO·Al_2O_3 was formed and most inclusions transformed to MnO−Al_2O_3−MgO type. As the initial Al content increased, the activity of Mg was further increased, and MgO inclusions were formed in steel. Finally, when the initial Al content further increased, Ca was reduced into the molten steel, and the inclusions were transformed into MnO−CaO−Al_2O_3−MgO and MnO−CaO−MgO type. According to previous research studies [29−31], the increase of Ca activity would cause MgO and MgO·Al_2O_3 inclusions to gradually become liquid inclusions. Thus, the shapes of the inclusions changed from spherical to irregular and finally to spherical with the increase of the initial Al content.

5. Conclusions

This study involved the investigation of the effect of the Al content on the reaction between Fe−10Mn−*x*Al (*x* = 0.035wt%, 0.5wt%, 1wt%, and 2wt%) steel and CaO−SiO_2−20wt%Al_2O_3−6wt%MgO (*B* = 4) slag at 1873 K. The main results are summarized as follows.

(1) After the slag/steel reaction, the Al content was significantly decreased. The initial Al content had a great effect on the composition of steel and slag. As the initial Al content increased from 0.035% to 2%, the Si content in steel gradually increased; whereas, SiO_2 and MnO contents in slag gradually decreased, and the Al_2O_3 content gradually increased.

(2) During the slag/steel reaction, Mn and Al in molten steel are two main reducing agents that reacted with top slag simultaneously. With the increase of the initial Al content, Al gradually replaced Mn to participate in slag/steel reaction. This process is the main reason for the composition change of steel and slag with the change of the initial Al content.

(3) As the initial content of Al increased from 0.035% to 2%, the types of inclusions changed greatly. The evolution route of inclusions was MnO → MnO−Al_2O_3−MgO → MgO → MnO−CaO−Al_2O_3−MgO and MnO−CaO−MgO. The evolution mechanism of inclusions was explored. With the increase of the initial Al content, Mg and Ca were reduced from top slag into molten steel in sequence, which consequently caused the transformation of inclusions.

(4) The shape of inclusions evolved from spherical to irregular, became faceted, and finally transformed to spherical. With the initial Al content increasing from 0.035% to 2%, the size of inclusions presented a trend that was increasing first and then decreasing.

Acknowledgements

This study was financially supported by the Ministry of Industry and Information Technology of China (No. TC180A6MR), China Scholarship Council and the National Natural Science Foundation of China (No. 51404020).

Conflict of Interest

The authors declare no conflict of interest.

References

[1] P. Von Schweinichen, Z.Y. Chen, D. Senk, and A. Lob, Effect of different casting parameters on the cleanliness of high manganese steel ingots compared to high carbon steel, *Metall. Mater. Trans. A*, 44(2013), No. 12, p. 5416.

[2] O. Grässel, L. Krüger, G. Frommeyer, and L.W. Meyer, High strength Fe–Mn–(Al, Si) TRIP/TWIP steels development — properties — application, *Int. J. Plast.*, 16(2000), No. 10-11, p. 1391.

[3] S.W. Hwang, J.H. Ji, and K.T. Park, Effects of Al addition on

high strain rate deformation of fully austenitic high Mn steels, *Mater. Sci. Eng. A*, 528(2011), No. 24, p. 7267.
[4] Y.J. Wang, S. Zhao, R.B. Song, and B. Hu, Hot ductility behavior of a Fe–0.3C–9Mn–2Al medium Mn steel, *Int. J. Miner. Metall. Mater.*, 28(2021), No. 3, p. 422.
[5] A. Dumay, J.P. Chateau, S. Allain, S. Migot, and O. Bouaziz, Influence of addition elements on the stacking-fault energy and mechanical properties of an austenitic Fe–Mn–C steel, *Mater. Sci. Eng. A*, 483-484(2008), p. 184.
[6] Y.J. Sutou, N. Kamiya, R. Umino, I. Ohnuma, and K. Ishida, High-strength Fe–20Mn–Al–C-based alloys with low density, *ISIJ Int.*, 50(2010), No. 6, p. 893.
[7] Z.J. Xie, C.J. Shang, X.L. Wang, X.M. Wang, G. Han, and R.D.K. Misra, Recent progress in third-generation low alloy steels developed under M^3 microstructure control, *Int. J. Miner. Metall. Mater.*, 27(2020), No. 1, p. 1.
[8] M. Koyama, T. Sawaguchi, K. Ogawa, T. Kikuchi, and M. Murakami, The effects of thermomechanical training treatment on the deformation characteristics of Fe–Mn–Si–Al alloys, *Mater. Sci. Eng. A*, 497(2008), No. 1-2, p. 353.
[9] K.G. Chin, C.Y. Kang, S.Y. Shin, S. Hong, S. Lee, H.S. Kim, K.H. Kim, and N.J. Kim, Effects of Al addition on deformation and fracture mechanisms in two high manganese TWIP steels, *Mater. Sci. Eng. A*, 528(2011), No. 6, p. 2922.
[10] J. Kim, S.J. Lee, and B.C. De Cooman, Effect of Al on the stacking fault energy of Fe–18Mn–0.6C twinning–induced plasticity, *Scripta Mater.*, 65(2011), No. 4, p. 363.
[11] A. Grajcar, U. Galisz, and L. Bulkowski, Non-metallic inclusions in high manganese austenitic alloys, *Arch. Mater. Sci. Eng.*, 50(2011), No. 1, p. 21.
[12] G. Gigacher, W. Krieger, P.R. Scheller, and C. Thomser, Non-metallic inclusions in high-manganese-alloy steels, *Steel Res. Int.*, 76(2005), No. 9, p. 644.
[13] J.H. Park, D.J. Kim, and D.J. Min, Characterization of non-metallic inclusions in high-manganese and aluminum-alloyed austenitic steels, *Metall. Mater. Trans. A*, 43(2012), No. 7, p. 2316.
[14] X.L. Xin, J. Yang, Y.N. Wang, R.Z. Wang, W.L. Wang, H.G. Zheng, and H.T. Hu, Effects of Al content on non-metallic inclusion evolution in Fe–16Mn–*x*Al–0.6C high Mn TWIP steel, *Ironmaking Steelmaking*, 43(2016), No. 3, p. 234.
[15] S.C. Chen, H.X. Ye, and X.Q. Lin, Effect of rare earth and alloying elements on the thermal conductivity of austenitic medium manganese steel, *Int. J. Miner. Metall. Mater.*, 24(2017), No. 6, p. 670.
[16] C.L. Zhuang, J.H. Liu, Z.L. Mi, H.T. Jiang, D. Tang, and G.X. Wang, Non-metallic inclusions in TWIP steel, *Steel Res. Int.*, 85(2014), No. 10, p. 1432.
[17] M. Peymandar, S. Schmuck, P. von Schweinichen, and D. Senk, Interfacial reactions between slag and melt in the new world of high manganese steels, [in] *Proc. of the TMS2014 Annual Meeting*, San Diego, 2014, p. 291.
[18] H.X. Yu, D.X. Yang, M.M. Li, and N. Zhang, Effects of Al addition on the reaction between high-manganese steel and CaO–SiO_2–Al_2O_3–MgO slag, *Steel Res. Int.*, 91(2020), No. 10, art. No. 2000143.
[19] D.J. Kim and J.H. Park, Interfacial reaction between CaO–SiO_2–MgO–Al_2O_3 flux and Fe–*x*Mn–*y*Al (*x* = 10 and 20 mass pct, *y* = 1, 3, and 6 mass pct) Steel at 1873 K (1600°C), *Metall. Mater. Trans. B*, 43(2012), No. 4, p. 875.
[20] Y.B. Kang, M.S. Kim, S.W. Lee, J.W. Cho, M.S. Park, and H.G. Lee, A reaction between high Mn–high Al steel and CaO–SiO_2–type molten mold flux: Part II. Reaction mechanism, interface morphology, and Al_2O_3 accumulation in molten mold flux, *Metall. Mater. Trans. B*, 44(2013), No. 2, p. 309.
[21] J. Park, S. Sridhar, and R.J. Fruehan, Kinetics of reduction of SiO_2 in SiO_2–Al_2O_3–CaO slags by Al in Fe–Al(–Si) melts, *Metall. Mater. Trans. B*, 45(2014), No. 4, p. 1380.
[22] H.X. Yu, D.X. Yang, M.M. Li, and M. Pan, Metallurgical characteristics of refining slag used for high manganese steel, *Metall. Res. Technol.*, 116(2019), No. 6, art. No. 620.
[23] Z.Y. Deng, L. Chen, G.D. Song, and M.Y. Zhu, Formation and evolution of non-metallic inclusions in Ti-bearing Al-killed steel during secondary refining process, *Metall. Mater. Trans. B*, 51(2020), No. 1, p. 173.
[24] H. Todoroki and K. Mizuno, Variation of inclusion composition in 304 stainless steel deoxidized with aluminum, *Iron Steelmaker*, 30(2003), No. 3, p. 60.
[25] Y.Q. Ji, C.Y. Liu, Y. Lu, H.X. Yu, F.X. Huang, and X.H. Wang, Effects of FeO and CaO/Al_2O_3 ratio in slag on the cleanliness of Al-killed steel, *Metall. Mater. Trans. B*, 49(2018), No. 6, p. 3127.
[26] M. Hino and K. Ito, *Thermodynamic Data for Steelmaking*, Tohoku University Press, Sendai, 2010, p. 24.
[27] K. Fujii, T. Nagasaka, and M. Hino, Activities of the constituents in spinel solid solution and free energies of formation of MgO, MgO Al_2O_3, *ISIJ Int.*, 40(2000), No. 11, p. 1059.
[28] H. Todoroki and K. Mizuno, Effect of silica in slag on inclusion compositions in 304 stainless steel deoxidized with aluminum, *ISIJ Int.*, 44(2004), No. 8, p. 1350.
[29] M. Jiang, X.H. Wang, B. Chen, and W.J. Wang, Laboratory study on evolution mechanisms of non-metallic inclusions in high strength alloyed steel refined by high basicity slag, *ISIJ Int.*, 50(2010), No. 1, p. 95.
[30] H.X. Yu, X.H. Wang, J. Zhang, and W.J. Wang, Characteristics and metallurgical effects of medium basicity refining slag on low melting temperature inclusions, *J. Iron Steel Res. Int.*, 22(2015), No. 7, p. 573.
[31] Y. Li, C.Y. Chen, G.Q. Qin, Z.H. Jiang, M. Sun, and K. Chen, Influence of crucible material on inclusions in 95Cr saw-wire steel deoxidized by Si-Mn, *Int. J. Miner. Metall. Mater.*, 27(2020), No. 8, p. 1083.